# Single Broadband Phase-Shaped Pulse Stimulated Raman Spectroscopy for Standoff Trace Explosive Detection

Rachel Glenn[†] and Marcos Dantus*[,†,‡]

[†]Department of Chemistry and [‡]Department of Physics and Astronomy, Michigan State University, East Lansing, Michigan 48824, United States

ABSTRACT: Recent success with trace explosives detection based on the single ultrafast pulse excitation for remote stimulated Raman scattering (SUPER-SRS) prompts us to provide new results and a Perspective that describes the theoretical foundation of the strategy used for achieving the desired sensitivity and selectivity. SUPER-SRS provides fast and selective imaging while being blind to optical properties of the substrate such as color, texture, or laser speckle. We describe the strategy of combining coherent vibrational excitation with a reference pulse in order to detect stimulated Raman gain or loss. A theoretical model is used to reproduce experimental spectra and to determine the ideal pulse parameters for best sensitivity, selectivity, and resolution when detecting one or more compounds simultaneously.

Selective Detection of

RDX trace on cotton at 7m
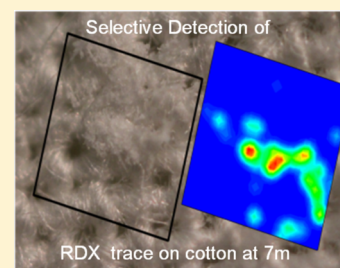
Despite years of research and development, standoff trace explosives detection (TED) continues to be a significant challenge waiting to be solved. Presently, the requirements can be summarized as the detection of single micrometer-sized particles of compounds with extremely low vapor pressure that are spread on a complex chemical background at a coverage quantified as submicrogram per cm^2 and from a distance greater than a few meters. The ideal system should be able to scan large areas and provide chemically resolved images that identify the explosive and its location in real time. Furthermore, the detection should be nondestructive, as well as eye- and skin-safe. Among the most promising advances in this field is single ultrafast pulse excited remote stimulated Raman scattering (SUPER-SRS),[1] illustrated in Figure 1, which has the potential to solve the TED challenge. The development of SUPER-SRS is part of ongoing efforts in our research group to take fundamental concepts from coherent control and nonlinear spectroscopy for improving practical applications such as pulse characterization,[2−5] biomedical imaging,[6−9] and chemical sensing.[1,10−12] Here, we provide a full description of SUPER-SRS, including a theoretical formalism that when coupled with numerical simulations allows us to predict signals, sensitivity, resolution, and multiple other characteristics as a function of source spectrum, intensity, and repetition rate. The theory is based upon perturbative expansion of the population element of the density matrix $\rho_{g_2 g_2}$ to fourth-order in the field, rather than the conventional technique of perturbative expansion of the polarization to third-order in the field. We use the new theory to simulate published and unpublished experimental results, and then, we show how this concept can be used to detect two or more explosives simultaneously.

The TED challenge is not new, and publications on the subject date back to the early 1970s.[13] International symposia on the subject started in 1983.[14] Since then, worldwide terrorism and asymmetric wars have highlighted the urgency of solving the TED challenge. The introduction provided and conclusions thereof are meant to briefly review this challenging field of research and development. Despite decades of effort more convenient and faster approaches that meet new safety levels required in public spaces and in the field remain to be developed. Approaches to TED can be separated into vapor detection or bulk detection. The main challenge of vapor detection is that most explosives have very low vapor pressures; for instance, while triacetone triperoxide (TATP) has a relatively high vapor pressure of $\sim 10^{-5}$ atm, 1,3,5-trinitroperhydro-1,3,5-triazine (RDX) has a vapor pressure of $\sim 10^{-12}$ atm,[15] making its detection in a complex and dusty atmosphere extremely challenging.

Bulk detection can be further divided into two approaches: the use of a swab to collect residues that can be analyzed by standard analytical approaches[16] and the use of lasers to detect residues at a distance.[17] Here, we focus on using lasers at distances greater than 1 m to detect explosives on a variety of surfaces ranging from car panels to clothing. We will not discuss approaches based on laser-induced fluorescence[18] because fluorescence from explosives or their photofragments is weak and broad, preventing sensitivity and selectivity. We will also not discuss laser-induced breakdown spectroscopy,[19] an approach that requires extensive fragmentation and ionization to yield atomic composition, therefore failing to provide sensitivity and selectivity in a nondestructive approach. Laser-induced absorption, particularly in the mid-IR, where vibrational bands can be excited is one viable approach. However, the temperature changes that would need to be recorded are too small for high-sensitivity detection in a wide variety of substrates. Therefore, tunable IR laser-based approaches have focused on utilizing pyrolysis following the laser excitation.[20] This leads us to Raman spectroscopy, which is capable of recording the vibrational spectrum of solid samples and has been explored since the early 1980s.[21,22]
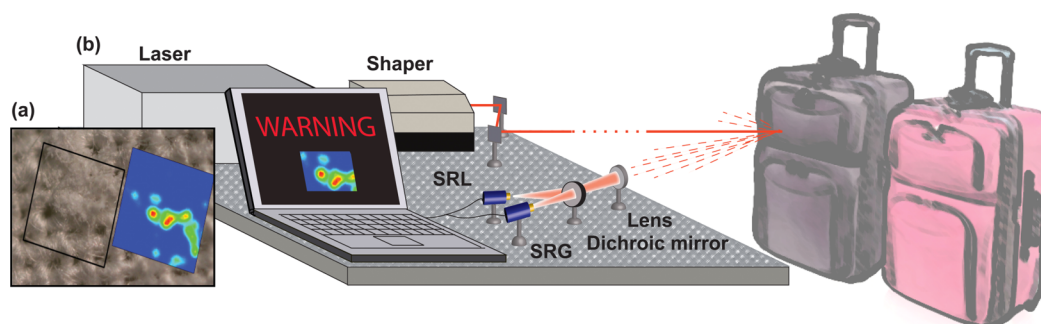
Figure 1. Illustration of the SUPER-SRS concept, experimental setup, and experimental results.[1] (a) Experimentally detected SUPER-SRS image of a trace quantity of RDX on cotton. A picture of the cotton fabric shows the micrometer-sized RDX particles, and the false color image of the 2×2 mm region delineated shows the corresponding SRS image. (b) Experimental setup showing the laser and the pulse shaper that creates two identical pulses, one for excitation and one for reference. Both collinear pulses are scanned on the target surface $3-7$ m from the scanning mirrors. The scattered light collected from the remote target is split between two fast photodiodes using a dichroic mirror to detect both stimulated Raman gain (SRG) and loss (SRL) simultaneously. The computer screen shows a warning due to a trace quantity of RDX that has been detected.

> The development of SUPER-SRS is part of ongoing efforts in our research group to take fundamental concepts from coherent control and nonlinear spectroscopy for improving practical applications.

Raman scattering is a spontaneous emission process at frequencies that correspond to the difference between the laser wavenumber and the wavenumber of the ith vibrational mode $(\tilde{\nu}_0 - \tilde{\nu}_i)$. The Raman cross section depends linearly on the laser power, concentration, path length, and collection angle. In addition, the number of Raman scattered photons depends on $\tilde{\nu}_0 (\tilde{\nu}_0 - \tilde{\nu}_i)^3$, the fourth power resulting from the instantaneous polarization of the molecules as in Rayleigh scattering. This dependence implies that the use of shorter-wavelength lasers enhances the Raman cross section. Furthermore, the Raman cross section is further enhanced by electronic resonance, where an additional resonance term is added to the denominator. Typical values for Raman cross sections are 10^{-29} cm^2 per molecule per steradian, a value that is at least 10 orders of magnitude smaller than the absorption cross section of molecules. The reader is referred to a dedicated reference for a more in-depth discussion of Raman cross sections.[23] The fourth-order dependence on photon energy and the electronic resonance enhancement provides a
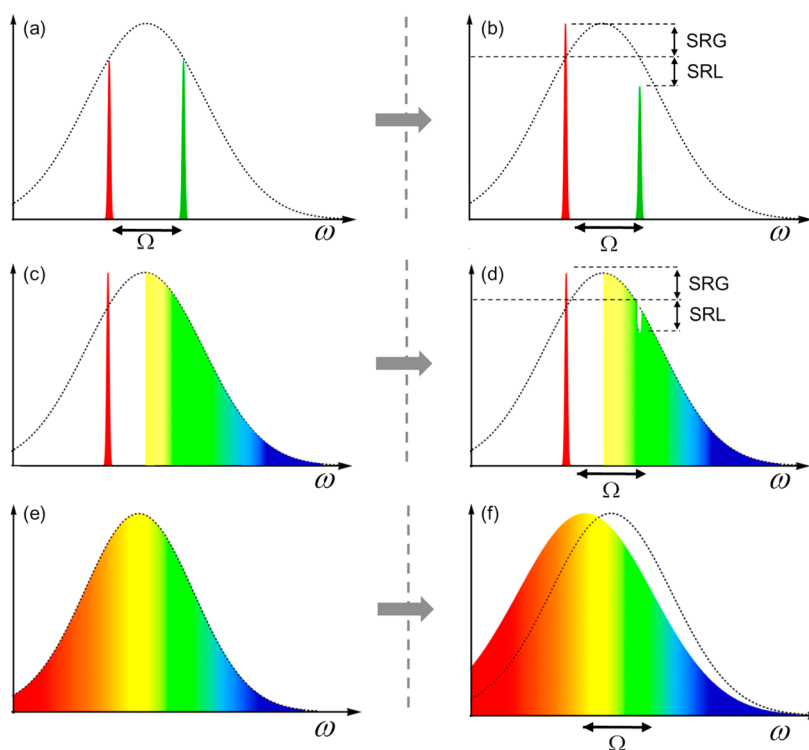

Figure 2. Illustrations of three conventional approaches for SRS (a,c,e) and their detected SRS signal (b,d,f): (a) two narrow broadband pulses; (c) a narrow band and a broadband pulse; (e) a single broadband pulse. The intensity difference between the two signals in b and d corresponds to the SRL and SRG signals.

significant opportunity to enhance Raman cross sections; this has led to significant activity in UV Raman-based TED approaches, especially at wavelengths shorter than 240 nm, where molecular fluorescence can be avoided.[24−27] The impressive success in this area is only tempered by the fact that resonance enhancement implies that analytes with different electronic states experience very different enhancements and that UV wavelengths may lead to photochemical degradation of both the analyte and substrate.

An alternative approach to enhancing Raman signals is to take advantage of the stimulated Raman scattering (SRS) enhancement, a process first discovered in 1962.[28] Similarly, lasers can stimulate the anti-Stokes Raman emission as in coherent anti-Stokes Raman scattering (CARS), a process first described in 1965.[29] Developments in laser technology over the last 50 years, enable at least three different approaches to stimulated Raman spectroscopy. One can combine a tunable and a fixed wavelength laser to detect a single Raman mode; use a narrow-band and a broadband laser to stimulate more than one vibrational mode at a time; or one can use a single broadband source to stimulate one or more vibrational modes at a time. Coherent stimulated Raman transitions are estimated to be 5 orders of magnitude greater than spontaneous Raman.[30]

Recent developments in coherent Raman spectroscopy and microscopy have led to significant improvements.[1,10−12,31−36] While a thorough review is beyond the scope of this Perspective, we highlight the development of single-beam CARS microscopy, whereby a single broadband laser pulse serves the purpose of pump, Stokes, and probe beam[31] and extensions of that approach serve for standoff detection of explosives.[1,11,32−34] Other notable work is the development of CARS microscopy with full spectral acquisition per pixel[35,36] and CARS imaging for flames.[37] From these developments, we favor SRS as used for microscopy[8] and as implemented for standoff detection.[1]

Here, we focus on SUPER-SRS because it can be used for vibrational-mode selective imaging at a rate limited only by the scan rate and laser repetition rate. The approach can also be used to collect a full Raman spectrum in order to confirm the detection of a particular explosive. SRS is not encumbered by nonresonant signals. Most importantly, the SRS signal is found in scattered light from the sample rather than as a coherent beam in CARS. This makes the location of the detector(s) much less important (see Figure 1). The technique discussed here in detail is one of many being tested in the laboratory, with recent efforts directed towards cost effectiveness and scalability.

Given that SUPER-SRS combines coherent spectroscopy with coherent control and time multiplexing, we develop a formalism to address each of these concepts separately. Then simulations of the SUPER-SRS signals are compared to experimentally measured spectra. Following the theory, we present time multiplexing, which allows SUPER-SRS to measure SRG and SRL from one or more analyte at the same time with very high sensitivity, even when using a noisy laser source.

Stimulated Raman Scattering. In conventional SRS spectroscopy, two narrow-band laser beams, pump and probe (Stokes) (Figure 2a), coincide on a sample. The presence of a Raman-active mode with energy that corresponds to the frequency difference between the two lasers causes the transfer of photons from the pump (higher frequency) to the Stokes or probe (lower frequency), as shown in Figure 2b. The loss in the pump signal (SRL) is detected by measuring the change in intensity at the blue-shifted wavelength, whereas the gain (SRG) is detected as the change in intensity detected at the red-shifted wavelength. SRG and SRL signals are free from nonresonant background. SRS

requires two synchronized laser pulses with at least one being tunable. Another option is to combine narrow- and broad-bandwidth pulses[38,39] (see Figure 2c) so that simultaneous detection of many Raman modes becomes possible. Illustration of the transfer of photons responsible for generating the SRL and SRG signals is shown in Figure 2d for a single Raman mode. In Figure 2e, a single broadband pulse is used as both the pump and Stokes pulses. In the detected signal, this creates a distribution of high-frequency photons being transferred to the lower-frequency side of the spectrum (Figure 2f), which may contain contributions from multiple Raman transitions within the bandwidth of the broadband laser. This approach greatly enhances sensitivity; however, spectral selectivity is lost unless the broadband pulse is shaped as discussed below.

SRS is a nonlinear process that can be described using time-dependent perturbation theory similar to CARS. Within this formalism, the SRS signal has been described using perturbation theory in the field−matter coupling by expanding the wave function or the density matrix. The signal is described by a third-order nonlinear optical susceptibility.[40−43] The associated diagrammatic representation is conventionally done using double-sided Feynman diagrams, such as the ones shown in Figure 3, for both CARS and SRS. In these diagrams, time flows
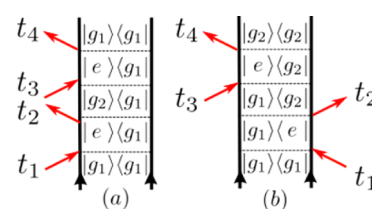

Figure 3. Feynman diagrams used to describe both SRS and CARS.

from bottom to top, and laser pulse interactions occur at times t_1, t_2, and t_3, with free evolution of the density matrix in between. The signal is emitted at time t_4. The evolution involves both the ground states g_1 and g_2 as well as off-resonance excitation of the electronic excited state(s) e. Off-resonance excitation, sometimes referred to as a transition through a virtual state, is possible because the light-matter interaction follows $\Delta E \Delta t \geq \hbar$ and for a very brief period of time the off-resonance excited state becomes accessible. Alternatively, the Lorentzian lineshape of all excited states extends well beyond resonance; the further off resonance the excitation laser is the shorter the interaction. This explains why virtual state excitation is considered an instantaneous process.

The diagram in Figure 3a corresponds to CARS processes and leads to an emission from the short-lived coherence eg_1 at time t_4. In CARS, the signal arises not only from the existence of a vibrational resonance with g_2 but also from a combination of the pulses in the absence of the vibrational resonance, the so-called nonresonant CARS component. The diagram in Figure 3b describes SRS. During the first two interactions with the field at t_1 and t_2, a vibrational coherence is formed involving g_1g_2. A similar process occurs on the other side of the diagram at times t_3 and t_4, leading to a population in g_2g_2. This implies that the SRS signal is proportional to the population of the excited vibrational state, that is, $\rho_{g_2g_2}$, which requires a transfer of photons from higher to lower frequencies. The SRL and SRG processes detected in SRS depend on Raman-mediated energy transfer and cannot occur unless there is a resonance within the bandwidth of the excitation
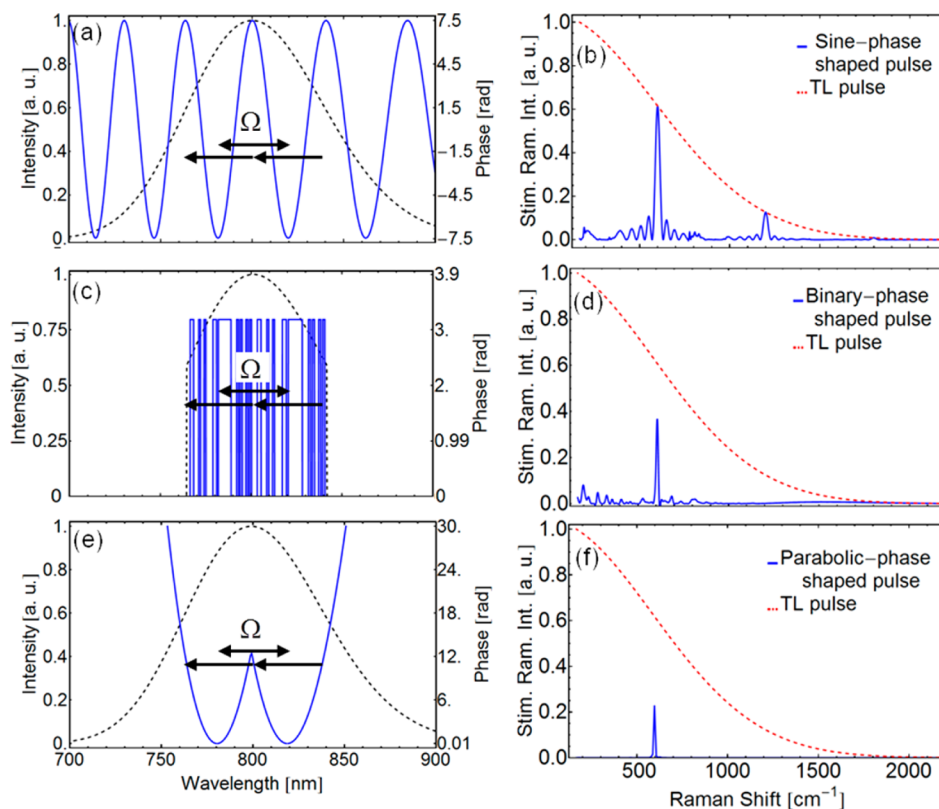
Figure 4. Illustrations of three different pulse-shaping functions for selective SRS excitation at a $\tilde{\nu}_\Omega = 600$ cm^{-1} (a,c,e) and their corresponding power spectrum from eq 6 as a function of Raman shift $\tilde{\nu}_{\omega_R}$ (b,d,f). The dashed red line in b, d and f corresponds to the power spectrum for a transform-limited Gaussian unshaped pulse. The dashed black line in a, c, and e is the Gaussian spectrum envelope. (a) Sine function; (c) binary phase function; (e) double parabolic (chirp) phase functions. Note that the three functions repeat with a frequency corresponding to the desired shift Ω; the symmetry of the phase is illustrated by the single arrows.

spectrum. Therefore, unlike CARS, SRL and SRG do not exhibit a nonresonant background.[44]

The time dependence of the density matrix element $\rho_{g_2g_2}$ can be calculated by perturbative expansion to fourth-order in the field. A similar approach was developed using transition probabilities,[45] where the CARS signal was described as the modulus squared of the transition probability to a vibrational mode by perturbatively expanding the wave functions. Here, we expand the density matrix perturbatively in the field–matter coupling to describe the SRS process as being proportional to the density matrix population $\rho_{g_2g_2}$. Overall, we arrive at a similar expression as that found via the transition amplitudes for CARS.[45]

The time evolution of the density matrix is expanded using the field–molecule coupling in the system Hamiltonian $\hat{H} = \hat{H}_0 + \hat{H}'$, where

$$\hat{H}_0 = \sum_{\nu=e_\nu,g_1} \hbar\omega_\nu |\nu\rangle\langle\nu| \tag{1}$$

represents the molecular system and $\hbar\omega_\nu$ is the energy of the state ν. The field–molecule interaction in the rotating wave approximation is

$$\hat{H}_{int} = -[\hat{E}^*(\mathbf{r}, t)V(t) + \hat{E}(\mathbf{r}, t)V^*(t)] \tag{2}$$

where the dipole lowering operator $V = \sum_{e,g_1} \mu_{g_1e}|g_1\rangle\langle e|$ is written in the interaction picture, $V(t) = U_0^\dagger(t,t_0)VU_0(t,t_0)$, where U_0 represents the evolution operator of the noninteracting Hamiltonian $\hat{H}_0$. The density matrix is given by $\rho(t) =$

$\sum_k P_k|\psi_k(t)\rangle\langle\psi_k(t)|$, where the individual matrix elements are given as $\rho_{nm}(t) = \sum_k P_k\langle n|\psi_k(t)\rangle\langle\psi_k(t)|m\rangle$. The time evolution of the density matrix is calculated perturbatively in $\hat{H}_{int}$ using the time evolution operator $U(t,t_0) = \exp_+[-(i/\hbar)\int_{t_0}^t d\tau\, \hat{H}'_{int}(\tau)]$, in the interaction picture, where $\hat{H}'_{int}(t) = U_0^\dagger(t,t_0)\hat{H}_{int}(t)U_0(t,t_0)$. The density matrix now reads

$$\rho_{nm}(t) = \sum_k P_k\langle n|U(t, t_0)|\psi_k(t_0)\rangle \times \langle\psi_k(t_0)|U^\dagger(t, t_0)|m\rangle \tag{3}$$

where U acting from the left propagates the ket and $U^\dagger$ acting from the right propagates the bra. Expanding U to second-order in $\hat{H}'_{int}$, the propagation of the ket correlation function can be written as

$$\langle n|U(t, t_0)|\psi_k(t_0)\rangle$$
$$= \langle n|\psi_k\rangle - \frac{i}{\hbar}\int_{t_0}^t d\tau\, \langle n|\hat{H}'_{int}(\tau)U(\tau, t_0)|\psi_k(t_0)\rangle \tag{4}$$

Expansion of the bra $\langle\psi_k(t_0)|U^\dagger(t,t_0)|m\rangle$ to second-order can be recognized as the complex conjugate of eq 4. The first term in the expansion in eq 4 gives the Kronecker's delta function. The second term can be interpreted as a transition probability from the state k to n along the ket. Note that the transition probability is zero for times $\tau > t$, so that we can extend the integration limits in eq 4 to infinity. Expansion of the right-hand side of eq 4 to first-order in $\hat{H}'_{int}(\tau)$ of the bra will lead to a SRS signal that is proportional to the square of the electric field, which is the linear contribution. The second-order expansion will lead to higher-order terms that give the nonlinear response. After expanding

both the bra and ket to second-order and multiplying them to calculate $\rho_{g_2g_2}$, the term proportional to fourth-order of the electric field is given as

$$\rho_{g_2g_2} \propto \left| -\frac{i}{2\pi\hbar^2} \sum_{g_2} \mu_{g_2e}\mu_{eg_1} \right.$$

$$\left. \times \int_{-\infty}^{+\infty} d\omega_1 \, d\omega_2 \, \frac{E^*(\omega_2)E(\omega_1)}{\omega_1 - \omega_e + i\eta} \delta(\omega_1 - \omega_2 - \omega_{g_2}) \right|^2$$

(5)

where $\omega_\nu = (1/\hbar)(\varepsilon_\nu - \varepsilon_{g_1})$. Here, we write the signal only in the frequency domain. This is more convenient because the detected spectrum is split into SRG and SRL spectral regions using a dichroic mirror. The definition of the SRS signal used in this Perspective is given by eq 5. The perturbative expansion using the Feynman diagram is shown in Figure 3b, where the bra and ket are both expanded to second-order in the electric field.

Selective Coherent Vibrational Excitation. Single-beam broadband Raman spectroscopy with high spectral resolution can be achieved with several different pulse-shaping techniques. Coherent control takes advantage of constructive and destructive interference between various quantum pathways connecting two states. For excitation of a Raman-active vibrational level with frequency Ω, the nonlinear power spectrum, which provides the field intensity at a frequency ω_R for the electric field given in eq 5, is given by

$$|E^*(\omega)E(\omega - \omega_R)|^2$$
$$= |\int A(\omega)A^*(\omega - \omega_R) \, e^{i\phi(\omega)-\phi(\omega-\omega_R)} \, d\omega|^2$$

(6)

Here, we inserted the definition of the field, $E(\omega) = A(\omega) \, e^{i\phi(\omega)}$, where $A(\omega)$ represents the field envelope, and $\phi(\omega)$ is the spectral phase of the pulse. Constructive interference occurs when the exponential phase cancels in eq 6, and destructive interference occurs when the phase minimizes eq 6. We note that there are various choices for the phase that will selectively and coherently drive the frequency Ω or in wavenumbers $\tilde{\nu}_\Omega = \Omega/2\pi c$. We discuss and compare three phase functions with Ω chosen to correspond to $\tilde{\nu}_\Omega = 600 \text{ cm}^{-1}$.

A sinusoidal phase function to selectively excite a single Raman mode was first demonstrated for single-beam CARS microscopy.[46] Figure 4a shows a Gaussian spectrum envelope (black dashed) and a sinusoidal phase function $\sin(\omega/2\pi\Omega)$ with frequency in wavenumbers of $\tilde{\nu}_\Omega = 600 \text{ cm}^{-1}$ (blue). The periodicity of the sine function splits the pulse in the time domain into a train of pulses with delay $\tau = 1/(\tilde{\nu}_\Omega c)$. As ω_R in eq 6 is scanned, a maximum occurs at Ω, as shown in Figure 4b (blue), where eq 6 is plotted using the field envelope and phase shown in Figure 4a. Note that the second harmonic of the desired frequency at $2\Omega = 1200 \text{ cm}^{-1}$ is also excited.

Cleaner excitation of a Raman transition can be accomplished by choosing a pseudorandom binary spectral phase function with 37 bits, $\phi(\omega) = \pi$ [0011000100100001101111111100010-1001011], with the total length corresponding to $\tilde{\nu}_\Omega = \tilde{\nu}_{\omega_R} = 600 \text{ cm}^{-1}$.[32,47] See Figure 4c. The binary phase repeats twice with a spacing equal to Ω, as shown in Figure 4c. The corresponding power spectrum as a function of ω_R in eq 6 is shown in Figure 4d. Note that the binary phase provides better selectivity without a contribution at 1200 cm^{-1} observed for a sinusoidal function.

By chirping a pair of laser pulses and carefully tuning their time delay $\tau = 2\pi/\Omega$, an enhancement of a single Raman mode has been demonstrated with CARS[48−50] and SRS.[51] A similar outcome can be accomplished with a single broadband pulse and two displaced parabolic spectral phase functions. Consider the two displaced parabolic phase functions and a broadband envelope shown in Figure 4e. The frequency shift Ω between the parabolas causes a peak in the power spectrum as a function of ω_R in eq 6. The stimulated power spectrum completely suppresses excitation at other frequencies, as shown in Figure 4f.

SUPER-SRS Signal. We described how SRS leads to a gain at lower frequencies and a loss at higher frequencies. We also described how a broadband pulse can be used to selectively excite at a designated range of frequencies. Those two concepts are now combined with a third concept. In order to determine if there has been gain or loss, one needs a reference pulse that in principle should be identical to the first in intensity and spectrum. SUPER-SRS uses two identical broadband pulses, an excitation and reference pulse, with a fixed time delay between them. The preparation of the reference pulse is described below. By subtraction of the reference signal from the excitation signal, one is able to detect gain or loss without the nonresonant background or any other optical differences such as absorption by the material or even laser speckle. See Figure 1 for illustration of the SUPER-SRS setup and detection of an experimentally detected RDX on a cotton chemical image. The experimental details are described in ref 1.

The coherent selection of the individual Raman mode is achieved with the phase function shown in Figure 4e

$$\phi(\omega) = \begin{cases} R\left(\omega - \left(\omega_0 - \frac{1}{2}\Omega\right)\right)^2 & \omega < \omega_0 \\ R\left(\omega - \left(\omega_0 + \frac{1}{2}\Omega\right)\right)^2 & \omega > \omega_0 \end{cases}$$

(7)

where Ω is the target mode and R is the chirp rate in units of fs^2. The spectral phase is inserted into eq 5. It is important to mention that the detected scattered light is split at $\lambda_L = 800$ nm using a dichroic mirror to detect the SRG and SRL simultaneously. The effect of the dichroic mirror on eq 5 is that it splits the integration into two regions, $<\omega_L$ and $>\omega_L$, which correspond to the SLG and SRL signals, respectively.

An analytical solution to the integration of eq 5 can be performed by approximating the broadband pulse envelope as a constant $A(\omega) = E_0$ in the frequency domain. Overall, this allows us to solve for the maximum theoretical resolution and obtain the frequency shift of the Raman resonance when an additional dispersion is added, as with the reference pulse. Under this assumption and for a single vibrational mode, the SRL signal for the excitation pulse, eq 5, can be cast into the following form

$$S_{exc}^{SRL}(\Omega) \propto \frac{E_0^4}{4\pi^2\hbar^4} |\mu_{g_2e}|^2 |\mu_{eg_1}|^2$$

$$\times \left| \int_{\omega_0}^{\omega_0+\omega_{g_2}} d\omega \frac{e^{-i\omega R(\Omega-\omega_{g_2})}}{\omega - \omega_e + i\eta} \right|^2$$

(8)

We assume that the laser frequency is tuned off-resonance from the electronic state e. Under this assumption, after evaluation of the integration, eq 8 can be cast into the form

$$S_{\text{exc}}^{\text{SRL}}(\Omega) \propto \frac{E_0^4}{4\pi^2\hbar^4} |\mu_{g_2 e}|^2 |\mu_{eg_1}|^2 \omega_{g_2}^2 \times \frac{\text{sinc}^2[R(\Omega - \omega_{g_2})\omega_{g_2}]}{(\omega_L - \omega_e)^2 + \eta^2}$$

$$(9)$$

The position of the Raman mode is located at $\Omega = \omega_{g_2}$, and it's corresponding line width, in units of wavenumbers, is given as

$$\Omega_{\text{FWHM}} = \frac{\alpha}{cR\omega_{g_2}} [\text{cm}^{-1}]$$

$$(10)$$

where c is the speed of light, $\alpha = \beta/\pi \approx 0.44$, and $\beta = \text{sinc}^{-1}(1/\sqrt{2})$ corresponds to the full width at half maximum (FWHM) of the sinc function. The Raman line width, eq 10, is plotted in Figure 5
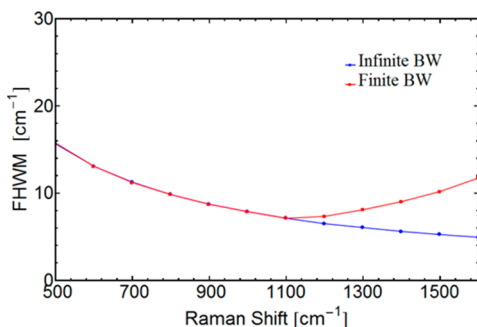

Figure 5. The linewidth FWHM of the Raman spectrum given by eq 9 as a function of ω_{g_2} as in eq 10, in units of wavenumbers, assuming that the laser pulse has infinite bandwidth (blue) or a bandwidth corresponding to 2270 cm^{-1} (red). The decrease in the FWHM for the narrow bandwidth occurs at one-half of the available bandwidth at 1135 cm^{-1} where the SRS signal has the highest intensity.

(blue) for a chirp $R = 10\,000$ fs^2. It can be seen that the line width decreases as its position increases. When the field envelope is included in eq 9, the line width and intensity of the individual peaks will be affected. The line width is plotted in Figure 5 for a square, 2270 cm^{-1} wide broadband pulse (red). The FWHM was calculated numerically. The line width follows eq 10 until one-half of the bandwidth; after that, the line width increases rather than decreases. This is because the Fourier transform of the sinc$^2(x)$ function is close to a triangular-shaped function. At one-half of the bandwidth, the Raman mode will have a maximum in intensity and will decrease linearly as the peak position increases or decreases. This increases the FWHM of the peak in the frequency domain.

Complete suppression of the background and any optical characteristics, such as absorption and reflectivity, is critical for detection of the SRL and SRG signals. Elimination of the dependence on optical characteristics in SUPER-SRS is done by subtracting the signal measured by the excitation pulse from the signal from the reference pulse, a pulse with identical spectrum and intensity to the excitation pulse but with a slightly different phase that detunes it from its resonance position. The reference pulse is prepared by first splitting the train of pulses into two identical pulses. A small additional linear chirp $C(\omega - \omega_C)^2$ is added to the reference beam in order to shift the spacing between the minima of the two parabolas in the spectral domain or equivalently to change their relative timing. The shift can be calculated using the same procedure as that for deriving eq 9

$$\Omega^{\text{Ref}} = \Omega\left(1 + \frac{C}{R}\right)$$

$$(11)$$

where we inserted $\omega_{g_2} = \Omega$. When detecting at a single Raman frequency, it is best to have a reference pulse with a Ω^{Ref} that is off-resonance with other Raman peaks. When scanning the excitation and reference pulses to obtain a SRS spectrum, two peaks are detected for each Raman-active vibrational mode, one from the excitation pulse and one from the reference pulse.

SUPER-SRS Simulations. The SUPER-SRS signal components SRL and SRG can be simulated by numerical evaluation of eq 5. The excitation and reference pulses are separated by 10 ns; therefore, calculation of the signal with the excitation pulse and reference pulse can be done separately. The SRL and SRG signal components are defined as the difference of the excitation signal and reference signal

$$S^{\text{SRL}} = S_{\text{exc}}^{\text{SRL}} - S_{\text{Ref}}^{\text{SRL}}$$

$$S^{\text{SRG}} = S_{\text{exc}}^{\text{SRG}} - S_{\text{Ref}}^{\text{SRG}}$$

$$(12)$$

In the Raman spectrum (S^{SRL} or S^{SRG}), there will be two vibrational mode lines, one positive at $\Omega = \omega_{g_2}$ from the excitation pulse and one negative given by eq 11 from the reference pulse. The line width of the vibrational mode depends on the bandwidth of the pulse; see eq 10 and Figure 5. The amplitude of the vibrational line will be at a maximum at one-half of the bandwidth and decrease with increasing/decreasing line position.

> Overall, the ability to detect two or more different explosive compounds simultaneously increases the speed of operation to provide fast screening.

Simulation of the SUPER-SRS experimentally measured signal of NH$_4$NO$_3$ at 1050 cm^{-1} is shown in Figure 6. The experimental
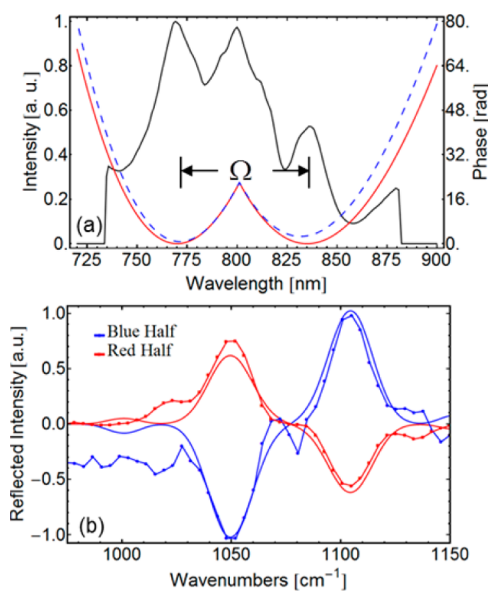

Figure 6. Experimental SUPER-SRS laser spectrum and spectral phase. (a) The excitation and reference pulse spectrum (black) and their corresponding phase (red and dashed blue). (b) The detected SRS signal, experimental (dotted−solid) and calculated (solid) for ammonium nitrate. The SRL signal is shown in blue, and the SRG signal is shown in red.

setup has been previously described.[1] The excitation pulse has an intensity spectrum (thin black line in Figure 6a) with a chirp rate of $R = 4000$ fs^2, and the reference pulse has additional chirp of $C = 205$ fs^2. The spectral phases of the excitation and reference pulses are shown in blue and dashed red in Figure 6a, respectively. The experimentally fitted SUPER-SRS signal is shown in Figure 6b. Both the SRL and SRG experimental data are well fitted by the simulation.

SUPER-SRS can be used to obtain a complete Raman spectrum of compounds with several vibrational modes by scanning the phase function. We demonstrate this in Figure 7 for (a) RDX and
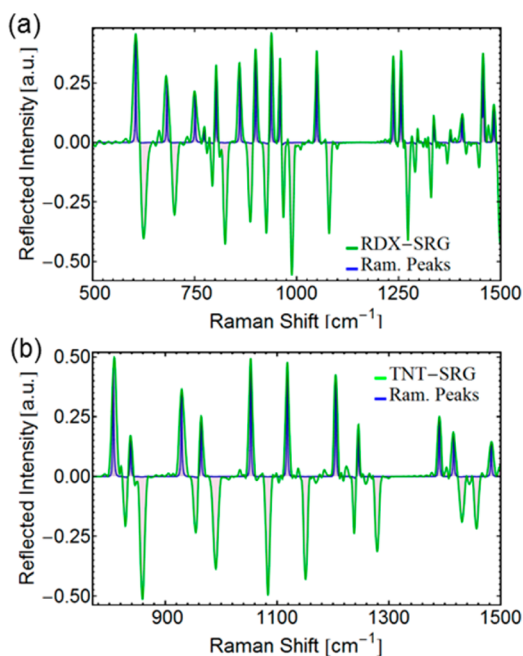

Figure 7. SUPER-SRS Raman spectrum for RDX (a) and TNT (b). The SRL signal is shown in green, and the Raman peak locations are highlighted in blue.

(b) trinitrotoluene (TNT), with a chirp rate of $R = 10\,000$ fs^2 and $C = 205$ fs^2. The SRG signal is shown in green. The Raman vibrational peak locations are highlighted with Lorentzian pulses in blue.

SUPER-SRS Detection of Multiple Compounds. The idea of individual selective Raman detection can be extended to detect two or more different explosives simultaneously by utilizing a multichirp selectivity or by adding time-delayed shaped pulses (from excitation and reference to multiple excitation pulses and one reference). For a multichirp approach, the spectral phase needs to be modified to include an additional chirp rate with a distance corresponding to the second Raman resonance. One possible choice for the phase is

$$\phi(\omega) = \begin{cases} R\left(\omega - \left(\omega_0 - \frac{1}{2}(\Omega_2 - \Omega_1)\right)\right)^2 & \omega < \omega_0 - \frac{1}{4}\Omega_2 \\ R\left(\omega - \left(\omega_0 - \frac{1}{2}\Omega_1\right)\right)^2 & \omega_0 - \frac{1}{4}\Omega_2 \le \omega \le \omega_0 \\ R\left(\omega - \left(\omega_0 + \frac{1}{2}\Omega_1\right)\right)^2 & \omega > \omega_0 \end{cases}$$

(13)

where Ω_1 and Ω_2 are the two selective Raman modes.

The overall concept of multicompound SUPER-SRS is illustrated in Figure 8. The laser can be thought of as a camera
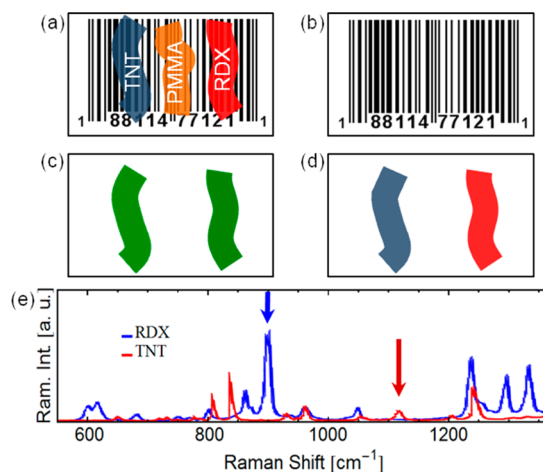

Figure 8. (a) Illustration of the strategy to simultaneously detect two types of explosives, TNT and RDX, deposited on a barcode; PMMA is also present but not detected because it is not resonant with the pulses used. (b) In the absence of a reference pulse, the system is unable to detect traces of the compounds. (c) The spectral phase is chosen to detect both Raman resonances at 900 cm^{-1} for RDX and 1118 cm^{-1} for TNT. (d) Illustration of the individual detection of the Raman modes at 900 cm^{-1} of RDX (red) and 1118 cm^{-1} of TNT (blue). (e) The Raman spectrm of RDX (blue) and TNT (red); the arrows show the vibrational modes chosen for detection.

used to scan surfaces, a barcode in this instance (Figure 8a). The barcode is simply chosen to highlight that SUPER-SRS is blind to changes in the optical properties of the substrate; it is only sensitive to Raman transitions of trace compounds on the substrate. In this approach, because both excitation and reference pulse trains are identical in intensity and spectrum and are perfectly collinear, it is insensitive to laser speckle. The barcode is contaminated with three different compounds: TNT, RDX, and poly(methyl methacrylate) (PMMA). PMMA represents a chemical background to which the laser is not sensitive. The spectral phase can be set for one or two types of explosive compounds, then the laser scans over the barcode to detect their presence. When the reference beam is blocked, no SRS signal is detected (Figure 8b), and the barcode is observed and overwhelms the SRS signals.

When the phase is set to selectively excite simultaneously two Raman modes[52] and a reference pulse is used, eq 13, both TNT and RDX can be detected during the raster scan. For example, from the spectrum shown in Figure 8e, one could choose $\Omega_1 = 1118$ cm^{-1} corresponding to TNT and $\Omega_2 = 900$ cm^{-1} corresponding to RDX. Figure 8c illustrates both RDX and TNT being detected simultaneously. A separate scan with the phase in eq 7 set to detect either RDX or TNT as in Figure 8d is required to image the location for each of the explosives. Overall, the ability to detect two or more different explosive compounds simultaneously increases the speed of operation to provide fast screening. If a compound of interest is detected, selective excitation or a Raman spectrum can be obtained at the specific location.

The development of novel coherent Raman strategies for standoff TED is of great importance. Here, we present new experimental data and give a full description of the SUPER-SRS strategy. The theoretical model describes the SRS signal, its

> The model presented here will aid in the development of additional strategies aimed at increasing the signal-to-noise ratio and optimizing detection of multiple different compounds.

quadratic dependence on laser intensity, and its linear dependence on a number of molecules. The relevant diagrams to allow identification of the density matrix elements and depict how signals depend on them, have been provided. The formalism is then used to successfully reproduce experimental SUPER-SRS data and to demonstrate additional capabilities of the approach such as acquisition of Raman spectra and simultaneous detection of two different compounds. Present experimental efforts are focused on increasing the imaging speed of this approach and implementing it on a 1550 nm fiber laser platform to make it practical and eye-safe. The model presented here will aid in the development of additional strategies aimed at increasing the signal-to-noise ratio and optimizing detection of multiple different compounds.

■ AUTHOR INFORMATION

Corresponding Author

*E-mail: dantus@msu.edu.

Notes

The authors declare no competing financial interest.

Biographies

Rachel Glenn is a postdoctoral researcher at Michigan State University. Glenn received her Ph.D. from M. E. Raikh and was a postdoctoral scholar with S. Mukamel, where she developed theory for multidimensional spectroscopy and intra- and intermolecular energy transfer in molecules, and now is focused on developing theory for larger molecules.

Marcos Dantus is the MSU Foundation Professor of Chemistry and University Distinguished Professor in Chemistry, Physics and Astronomy at Michigan State University. Dantus, a Member of the National Academy of Inventors, is known for pioneering work in Femtochemistry, four-wave mixing, and his contributions to pulse shaping and coherent control.

■ ACKNOWLEDGMENTS

■ REFERENCES

(1) Bremer, M. T.; Dantus, M. Standoff Explosives Trace Detection and Imaging by Selective Stimulated Raman Scattering. *Appl. Phys. Lett.* **2013**, *103*, 061119.

(2) Dantus, M.; Lozovoy, V. V. Experimental Coherent Laser Control of Physicochemical Processes. *Chem. Rev.* **2004**, *104*, 1813−1860.

(3) Xu, B. W.; Gunn, J. M.; Dela Cruz, J. M.; Lozovoy, V. V.; Dantus, M. Quantitative Investigation of the Multiphoton Intrapulse Interference Phase Scan Method for Simultaneous Phase Measurement and Compensation of Femtosecond Laser Pulses. *J. Opt. Soc. Am. B* **2006**, *23*, 750−759.

(4) Coello, Y.; Lozovoy, V. V.; Gunaratne, T. C.; Xu, B.; Borukhovich, I.; Tseng, C.-h.; Weinacht, T.; Dantus, M. Interference without an Interferometer: A Different Approach to Measuring, Compressing, and Shaping Ultrashort Laser Pulses. *J. Opt. Soc. Am. B* **2008**, *25*, A140−A150.

(5) Lozovoy, V. V.; Rasskazov, G.; Pestov, D.; Dantus, M. Quantifying Noise in Ultrafast Laser Sources and its Effect on Nonlinear Applications. *Opt. Express* **2015**, *23*, 12037−12044.

(6) Dela Cruz, J. M.; Pastirk, I.; Comstock, M.; Lozovoy, V. V.; Dantus, M. Use of Coherent Control Methods Through Scattering Biological Tissue to Achieve Functional Imaging. *Proc. Natl. Acad. Sci. U. S. A.* **2004**, *101*, 16996−17001.

(7) Xi, P.; Andegeko, Y.; Pestov, D.; Lovozoy, V. V.; Dantus, M. Two-photon Imaging using Adaptive Phase Compensated Ultrashort Laser Pulses. *J. Biomed. Opt.* **2009**, *14*, 014002.

(8) Freudiger, C. W.; Min, W.; Holtom, G. R.; Xu, B.; Dantus, M.; Xie, X. S. Highly Specific Label-Free Molecular Imaging with Spectrally Tailored Excitation-Stimulated Raman Scattering (STE-SRS) Microscopy. *Nat. Photonics* **2011**, *5*, 103−109.

(9) Nie, B.; Saytashev, I.; Chong, A.; Liu, H.; Arkhipov, S. N.; Wise, F. W.; Dantus, M. Multimodal Microscopy with Sub-30 fs Yb Fiber Laser Oscillator. *Biomed. Opt. Express* **2012**, *3*, 1750−1756.

(10) Li, H.; Harris, D. A.; Xu, B.; Wrzesinski, P. J.; Lozovoy, V. V.; Dantus, M. Coherent Mode-Selective Raman Excitation Towards Standoff Detection. *Opt. Express* **2008**, *16*, 5499−5504.

(11) Li, H.; Harris, D. A.; Xu, B.; Wrzesinski, P. J.; Lozovoy, V. V.; Dantus, M. Standoff and Arms-Length Detection of Chemicals with Single-Beam Coherent Anti-Stokes Raman Scattering. *Appl. Opt.* **2009**, *48*, B17−22.

(12) Bremer, M. T.; Wrzesinski, P. J.; Butcher, N.; Lozovoy, V. V.; Dantus, M. Highly Selective Standoff Detection and Imaging of Trace Chemicals in a Complex Background using Single-Beam Coherent Anti-Stokes Raman Scattering. *Appl. Phys. Lett.* **2011**, *99*, 101109.

(13) Washington, W. D.; Midkiff, C. R., Jr. Systematic Approach to the Detection of Explosive Residues. II Trace Vapor Analysis. *J. Assoc. Offic. Anal. Chemists* **1973**, *56*, 1239.

(14) *Proceedings of the International Symposium on the Analysis and Detection of Explosives*; FBI Academy: Quantico, VA, 1983.

(15) The vapor pressure of explosives. *TrAC, Trends Anal. Chem.* **2013**, *42*, 1−228.10.1016/j.trac.2012.11.002

(16) Douse, J. M. F. Trace Analysis of Explosives in Handswab Extracts Using Amberlite XAD-7 Porous Polymer Beads, Silica Capillary Column Gas Chromatography with Electron-Capture Detection and Thin-Layer Chromatography. *J. Chromatogr. A* **1982**, *234*, 415−425.

(17) Haley, L. V.; Hallowell, S. F. Laser Based Explosives Detection. *Proceedings of the IEEE 34th Annual 2000 International Carnahan Conference on Security Technology*; 2000; pp 207−217.

(18) Wu, D.; Singh, J. P.; Yueh, F. Y.; Monts, D. L. 2,4,6-Trinitrotoluene Detection by Laser-Photofragmentation-Laser-Induced Fluorescence. *Appl. Opt.* **1996**, *35*, 3998−4003.

(19) Harmon, R. S.; De Lucia, F. C.; Winkel, R. J., Jr.; LaPointe, A.; Grossman, S. L.; McNesby, K. L.; Miziolek, A. W. LIBS: A New Versatile, Field Deployable, Real-Time Detector System with Potential for Landmine Detection. *Proc. SPIE* **2003**, *5089*, 1065−1077.

(20) Wormhoudt, J.; Shorter, J. H.; McManus, J. B.; Kebabian, P. L.; Zahniser, M. S.; Davis, W. M.; Cespedes, E. R.; Kolb, C. E. Tunable Infrared Laser Detection of Pyrolysis Products of Explosives in Soils. *Appl. Opt.* **1996**, *35*, 3992−3997.

(21) Carver, F. W. S.; Sinclair, T. J. Spectroscopic Studies of Explosives: 1—Detection of Nitro Compounds on Silica Gel and Carbon by Non-Resonant Raman Spectroscopy. *J. Raman Spectrosc.* **1983**, *14*, 410−414.

(22) Trott, W. M.; Renlund, A. M. Single-Pulse Raman Scattering Studies of Heterogeneous Explosive Materials. *Appl. Opt.* **1985**, *24*, 1520.

(23) McCreery, R. L. Photometric Standards for Raman Spectroscopy. In *Handbook of Vibrational Spectroscopy*; Chalmers, J. M., Griffiths, P. R., Eds.; John Wiley & Sons, Ltd: New York, 2006.

(24) Asher, S.; Johnson, C. Raman-Spectroscopy of a Coal Liquid Shows That Fluorescence Interference. *Science* **1984**, *225*, 311−313.

(25) Storrie-Lombardi, M. C.; Hug, W. F.; McDonald, G. D.; Tsapin, A. I.; Nealson, K. H. Hollow Cathode Ion Lasers for Deep Ultraviolet Raman Spectroscopy and Fluorescence Imaging. *Rev. Sci. Instrum.* **2001**, *72*, 4452−4459.

(26) Tuschel, D. D.; Mikhonin, A. V.; Lemoff, B. E.; Asher, S. A. Deep Ultraviolet Resonance Raman Excitation Enables Explosives Detection. *Appl. Spectrosc.* **2010**, *64*, 425−432.

(27) Bhartia, R.; Hug, W. F.; Reid, R. D. Improved Sensing Using Simultaneous Deep UV Raman and Fluorescence Detection. *Proc. SPIE 8358, Chemical, Biological, Radiological, Nuclear, and Explosives (CBRNE) Sensing XIII, 83581A*; 2012; pp 83581A/1−83581A/9.

(28) Eckhardt, G.; Hellwarth, R. W.; McClung, F. J.; Schwarz, S. E.; Weiner, D.; Woodbury, E. J. Stimulated Raman Scattering From Organic Liquids. *Phys. Rev. Lett.* **1962**, *9*, 455−457.

(29) Maker, P. D.; Terhune, R. W. Study of Optical Effects Due to an Induced Polarization Third Order in the Electric Field Strength. *Phys. Rev.* **1965**, *137*, A801−A818.

(30) Pestov, D.; Ariunbold, G. O.; Wang, X.; Murawski, R. K.; Sautenkov, V. A.; Sokolov, A. V.; Scully, M. O. Coherent Versus Incoherent Raman Scattering: Molecular Coherence Excitation and Measurement. *Opt. Lett.* **2007**, *32*, 1725−1727.

(31) Oron, D.; Dudovich, N.; Silberberg, Y. Single-Pulse Phase-Contrast Nonlinear Raman Spectroscopy. *Phys. Rev. Lett.* **2002**, *89*, 273001.

(32) Dantus, M.; Li, H.; Harris, D. A.; Xu, B.; Wrzesinski, P. J.; Lozovoy, V. V. Detection of Chemicals at a Standoff > 10 m Distance Based on Single-Beam Coherent Anti-Stokes Raman Scattering. In *Chemical, Biological, Radiological, Nuclear, and Explosives (cbrne) Sensing IX*, Fountain, A. W., III, Gardner, P. J., Eds.; Spie-Int Soc Optical Engineering: Bellingham, WA, 2008; Vol. *6954*, p 69540P.

(33) Katz, O.; Natan, A.; Silberberg, Y.; Rosenwaks, S. Standoff Detection of Trace Amounts of Solids by Nonlinear Raman Spectroscopy using Shaped Femtosecond Pulses. *Appl. Phys. Lett.* **2008**, *92*, 171116.

(34) Natan, A.; Levitt, J. M.; Graham, L.; Katz, O.; Silberberg, Y. Standoff Detection via Single-Beam Spectral Notch Filtered Pulses. *Appl. Phys. Lett.* **2012**, *100*, 051111.

(35) Hartshorn, C. M.; Lee, Y. J.; Camp, C. H.; Liu, Z.; Heddleston, J.; Canfield, N.; Rhodes, T. A.; Walker, A. R. H.; Marsac, P. J.; Cicerone, M. T. Multicomponent Chemical Imaging of Pharmaceutical Solid Dosage Forms with Broadband CARS Microscopy. *Anal. Chem.* **2013**, *85*, 8102−8111.

(36) Camp, C. H., Jr.; Lee, Y. J.; Heddleston, J. M.; Hartshorn, C. M.; Walker, A. R. H.; Rich, J. N.; Lathia, J. D.; Cicerone, M. T. High-Speed Coherent Raman Fingerprint Imaging of Biological Tissues. *Nat. Photonics* **2014**, *8*, 627−634.

(37) Bohlin, A.; Kliewer, C. J. Communication: Two-Dimensional Gas-Phase Coherent Anti-Stokes Raman Spectroscopy (2D-CARS): Simultaneous Planar Imaging and Multiplex Spectroscopy in a Single Laser Shot. *J. Chem. Phys.* **2013**, *138*, 221101.

(38) Lim, S.-H.; Caster, A. G.; Leone, S. R. Fourier Transform Spectral Interferometric Coherent Anti-Stokes Raman Scattering (FTSI-CARS) Spectroscopy. *Opt. Lett.* **2007**, *32*, 1332−1334.

(39) Ploetz, E.; Laimgruber, S.; Berner, S.; Zinth, W.; Gilch, P. Femtosecond Stimulated Raman Microscopy. *Appl. Phys. B: Lasers Opt.* **2007**, *87*, 389−393.

(40) Shen, Y. R. *The Principles of Nonlinear Optics*; Wiley: New York, 1984; p 584.

(41) Rahav, S.; Roslyak, O.; Mukamel, S. Manipulating Stimulated Coherent Anti-Stokes Raman Spectroscopy Signals by Broad-Band and Narrow-Band Pulses. *J. Chem. Phys.* **2009**, *131*, 194510.

(42) Cheng, J.-X.; Xie, X. S. *Coherent Raman Scattering Microscopy*; CRC Press: Boca Raton, FL, 2012; p 613.

(43) Brown, E. J.; Zhang, Q.; Dantus, M. Femtosecond Transient-Grating Techniques: Population and Coherence Dynamics Involving Ground and Excited States. *J. Chem. Phys.* **1999**, *110*, 5772−5788.

(44) Freudiger, C. W.; Min, W.; Saar, B. G.; Lu, S.; Holtom, G. R.; He, C.; Tsai, J. C.; Kang, J. X.; Xie, X. S. Label-Free Biomedical Imaging with High Sensitivity by Stimulated Raman Scattering Microscopy. *Science* **2008**, *322*, 1857−1861.

(45) Rahav, S.; Mukamel, S. Stimulated Coherent Anti-Stokes Raman Spectroscopy (CARS) Resonances Originate from Double-Slit Interference of Two-Photon Stokes Pathways. *Proc. Natl. Acad. Sci. U. S. A.* **2010**, *107*, 4825−4829.

(46) Dudovich, N.; Oron, D.; Silberberg, Y. Single-Puse Coherently Controlled Nonlinear Raman Spectroscopy and Microscopy. *Nature* **2002**, *418*, 512−514.

(47) Lozovoy, V. V.; Xu, B.; Shane, J. C.; Dantus, M. Selective Nonlinear Optical Excitation with Pulses Shaped by Pseudorandom Galois Fields. *Phys. Rev. A: At., Mol., Opt. Phys.* **2006**, *74*, 041805.

(48) Gershgoren, E.; Bartels, R. A.; Fourkas, J. T.; Tobey, R.; Murnane, M. M.; Kapteyn, H. C. Simplified Setup for High-Resolution Spectroscopy that uses Ultrashort Pulses. *Opt. Lett.* **2003**, *28*, 361−363.

(49) Malinovskaya, S. A.; Malinovsky, V. S. Chirped-Pulse Adiabatic Control in Coherent Anti-Stokes Raman Scattering for Imaging of Biological Structure and Dynamics. *Opt. Lett.* **2007**, *32*, 707−709.

(50) Pegoraro, A. F.; Ridsdale, A.; Moffatt, D. J.; Jia, Y.; Pezacki, J. P.; Stolow, A. Optimally Chirped Multimodal CARS Microscopy Based on a Single Ti:Sapphire Oscillator. *Opt. Express* **2009**, *17*, 2984−2996.

(51) Fu, D.; Holtom, G.; Freudiger, C.; Zhang, X.; Xie, X. S. Hyperspectral Imaging with Stimulated Raman Scattering by Chirped Femtosecond Lasers. *J. Phys. Chem. B* **2013**, *117*, 4634−4640.

(52) Li, H.; Harris, D. A.; Xu, B.; Wrzesinski, P. J.; Lozovoy, V. V.; Dantus, M. Single-Beam Coherent Anti-Stokes Raman Scattering for Standoff Detection. *Opt. Photonics News* **2008**, *19*, 46−46.